

# An Asymptotic Preserving Discrete Velocity Method based on Exponential Bhatnagar-Gross-Krook Integration

F. Garmirian<sup>1, a)</sup> and M. Pfeiffer<sup>1, b)</sup>

*Institute of Space Systems, University of Stuttgart, Pfaffenwaldring 29, 70569 Stuttgart, Germany*

(Dated: 14 August 2023)

The Bhatnagar-Gross-Krook (BGK) model of the Boltzmann equation allows for efficient flow simulations, especially in the transition regime between continuum and high rarefaction. However, ensuring efficient performances for multiscale flows, in which the Knudsen number varies by several orders of magnitude, is never straightforward. Discrete velocity methods as well as particle-based solvers can each reveal advantageous in different conditions, but not without compromises in specific regimes. This article presents a second-order asymptotic preserving discrete velocity method to solve the BGK equation, with the particularity of thoroughly maintaining positivity when operations are conducted on the distribution function. With this procedure based on exponential differencing, it is therefore also possible to construct an adapted version of this second-order method using the stochastic particle approach, as presented in Pfeiffer, Garmirian, and Gorji<sup>1</sup>. The deterministic variant is detailed here and its performances are evaluated on several test cases. Combined to the probabilistic solver and with the possibility of a future coupling, our exponential differencing discrete velocity method provides a robust toolbox that would be useful in efficiently simulating multiscale gas phenomena.

## I. INTRODUCTION

In recent years, a variety of gas kinetic methods allowing for efficient multiscale non-equilibrium simulations have been developed. Different classifications of such methods can be introduced. One possible classification is the division between mostly deterministic methods in Euler formulation, i.e. on a fixed grid<sup>2-4</sup>, and mostly stochastic methods in Lagrange formulation, i.e. on a moving grid, which are usually also referred to as particle methods<sup>5-11</sup>, with some methods combining both representations<sup>12</sup>. Within the methods in the Euler formulation, the unified gas kinetic scheme<sup>3</sup> (UGKS) and discrete unified gas kinetic scheme<sup>2,13,14</sup> (DUGKS) as special forms of the discrete velocity method<sup>4</sup> (DVM) have made great progress in the efficient simulation of multiscale problems in recent years. The special feature of both methods is that they show asymptotic preserving (AP) behaviour. The time step size is thus not limited to the relaxation time due to the implicit treatment of the collision operator (here a Bhatnagar-Gross-Krook operator). Besides, for small Knudsen numbers the behaviour of the Chapman-Enskog expansion is preserved and the methods are at least second-order accurate in both the free-molecular regime and the continuum regime. The implicit treatment of the collision term is realised by a Crank-Nicolson integration, which can be written down again in an explicit form by clever variable transformation, resulting in a particularly efficient method<sup>2,3</sup>.

For the particle methods on the other hand, there have also been efforts in recent years to construct AP methods. The idea is also to replace the collision term of the complicated Boltzmann equation with simpler approximations. These are either the BGK collision operator<sup>1,5-8</sup> or the Fokker-Planck

operator<sup>15-17</sup>. In the case of the BGK operator in particular, the idea is to use the approach from the DUGKS method with the Crank-Nicolson integration and transfer it to the particles. However, since in this approach the pre-factors of the integration can take on any (positive and negative) values, as shown in Section II B, this approach is not easily transferable to particle methods.

One solution to this problem is the USP-BGK method<sup>7,8</sup>. Here, an additional collision term was inserted in which the current distribution function is approximated by a Grad-13 approximation<sup>18</sup>. This allows the advection and the relaxation process to be solved together which is a requirement for the construction of AP methods. The choice of the Grad-13 distribution also ensures that the Navier-Stokes limit is asymptotically preserved. This additional collision term is constructed to satisfy the Navier-Stokes equations in the continuum domain with a second-order time integration. In the case of large Knudsen numbers, however, the method falls back to first order. An approach that leads to a second-order particle method in both rarefied and continuum regimes was recently presented in the form of the exponential integration of the BGK equation<sup>1</sup>. With this method, thanks to certain pre-factors as the result of implicit integration, it is very easy to construct particle processes that always have positive particle weights and AP behaviour.

In this article, this exponential integration approach will be used to construct an AP-DVM method similar to DUGKS. The idea of exponential integration has been successfully used in the past to construct asymptotic preserving Runge-Kutta methods of second order<sup>19</sup> or even higher order for the BGK equation<sup>20-22</sup>. The special feature of the integrator presented here is that it has then the exact same integration approach and behavior as the particle method. In the future, it will hopefully be possible to easily couple the DVM approach and the particle approach in order to be able to use the advantages of both approaches in the flow simulations. This idea is already used in the Discrete Unified Gas-Kinetic Wave-Particle

<sup>a)</sup>Electronic mail: garmirianf@irs.uni-stuttgart.de (corresponding author)

<sup>b)</sup>Electronic mail: mpfeiffer@irs.uni-stuttgart.de

method<sup>12</sup> to combine the advantages of DVM and particle methods. Here, however, we would have the first approach in which both methods can be integrated identically and equally in time, hopefully making the coupling and the coupling behaviour easier.

This article begins with an overview of the BGK approximation and a summary of the DUGKS method in order to go into the problem of the pre-factors again. Then the derivation and implementation of the exponential integrator method for the DVM approach is shown, followed by various validation cases.

## II. THEORY

### A. BGK approximation

The basis for the kinetic description of gases is the Boltzmann equation

$$\frac{\partial f}{\partial t} + \mathbf{v} \cdot \frac{\partial f}{\partial \mathbf{x}} = \frac{\partial f}{\partial t} \Big|_{\text{coll}}, \quad (1)$$

given here in the monatomic case, where the distribution function  $f(\mathbf{x}, \mathbf{v}, t)$  depends on time  $t$ , particle velocity  $\mathbf{v}$  and position  $\mathbf{x}$ .

The BGK model<sup>23</sup> approximates the collision term by making the distribution function  $f$  relax towards a target distribution  $f^t$ , with a certain relaxation frequency  $\nu$ :

$$\frac{\partial f}{\partial t} \Big|_{\text{coll}} = \nu(f^t - f) = \Omega. \quad (2)$$

A first choice of target would be a simple Maxwellian distribution

$$f^M = \rho \left( \frac{1}{2\pi RT} \right)^{3/2} \exp \left[ -\frac{\mathbf{c} \cdot \mathbf{c}}{2RT} \right], \quad (3)$$

with density  $\rho$ , temperature  $T$ , specific gas constant  $R$  and the thermal velocity  $\mathbf{c} = \mathbf{v} - \mathbf{u}$ , where  $\mathbf{u}$  is the average flow velocity. The relaxation frequency is chosen so as to give rise to the intended viscosity  $\mu = \frac{\rho RT}{\nu}$ . However, this leads to a fixed Prandtl number  $\text{Pr} = 1$ . To obtain a correct Prandtl number ( $2/3$  for a monatomic ideal gas), one option is the Shakhov model<sup>24</sup>. In this model, the heat flux  $\mathbf{q} = \frac{1}{2} \int \mathbf{c}(\mathbf{c} \cdot \mathbf{c}) f d\mathbf{v}$  is used to modify the target distribution in order to accurately account for viscous and thermal effects at the same time:

$$f^S = f^M \left[ 1 + (1 - \text{Pr}) \frac{\mathbf{c} \cdot \mathbf{q}}{5\rho(RT)^2} \left( \frac{\mathbf{c}^2}{RT} - 5 \right) \right]. \quad (4)$$

The Shakhov distribution is always chosen in the rest of this article, but the described method could be applied to any conservative BGK-based model with modified target distribution.

### B. Recap of the Discrete Unified Gas Kinetic Scheme

The idea behind the DUGKS is to construct an asymptotic preserving integration method to solve the BGK equation with

second-order accuracy<sup>2,13</sup>. For this, the velocity space is discretized using appropriate quadratures (see Section III A), resulting in a DVM approach where the problem is converted to  $N$  equations with fixed velocity  $\mathbf{v} \in (\mathbf{v}_i)_{i \in [1, N]}$ . Then, one integrates the collision operator of the BGK equation (2) with a Crank-Nicolson scheme and applies the midpoint rule to the flux  $\mathcal{F} = \mathbf{v} \cdot \frac{\partial f}{\partial \mathbf{x}}$ :

$$f(\mathbf{x} + \mathbf{v}\Delta t, \mathbf{v}, t + \Delta t) = f(\mathbf{x}, \mathbf{v}, t) + \mathcal{F}(t + \Delta t/2) + \frac{\Delta t}{2} (\Omega(\mathbf{x} + \mathbf{v}\Delta t, \mathbf{v}, t + \Delta t) + \Omega(\mathbf{x}, \mathbf{v}, t)). \quad (5)$$

By cleverly rearranging the terms and introducing the two new variables

$$\tilde{f} = f - \frac{\Delta t}{2} \Omega = \frac{2\tau + \Delta t}{2\tau} f - \frac{\Delta t}{2\tau} f^t \quad (6)$$

$$\text{and } \hat{f} = f + \frac{\Delta t}{2} \Omega = \frac{2\tau - \Delta t}{2\tau} f + \frac{\Delta t}{2\tau} f^t, \quad (7)$$

with  $\tau = 1/\nu$  being the relaxation time, it is possible to eliminate the stiffness of the collision operator by treating it implicitly:

$$\tilde{f}(\mathbf{v}, \mathbf{x} + \mathbf{v}\Delta t, t + \Delta t) = \hat{f}(\mathbf{v}, \mathbf{x}, t) + \mathcal{F}(t + \Delta t/2). \quad (8)$$

With a suitable construction of the flux term  $\mathcal{F}$ , it is thus possible to achieve an implicit integration of the coupled advection and relaxation. However, for stochastic particle methods, the pre-factors that occur in equations (6)-(7) become a problem. Since these can become negative at large time steps relative to the relaxation time and because these pre-factors are interpreted as the probability of the individual particles (see Pfeiffer, Garmirian, and Gorji<sup>1</sup>), this leads to major problems in the adaptation to particle methods. In the following, the construction of an integration method with unconditionally positive pre-factors, which are also always limited to  $[0; 1]$ , is described. It can then be used directly as a DVM, but also as a stochastic particle method.

### C. Exponential time differencing BGK

In order to construct a second-order multiscale DVM, the stiffness induced in the BGK equation when the relaxation frequency  $\nu$  increases needs to be addressed. The approach followed here is the same as used in Pfeiffer, Garmirian, and Gorji<sup>1</sup>, where particular attention is paid to the positivity of pre-factors in order to build a particle-based solver. An exact integration of the BGK equation is first conducted using exponential time differencing, which is particularly advantageous to handle a stiff linear term in ordinary differential equations<sup>25</sup>:

$$f(t^{n+1}) = f(t^n) e^{-\nu \Delta t} + e^{-\nu \Delta t} \int_0^{\Delta t} e^{\nu s} \left( \nu f^t(t^n + s) - \mathbf{v} \cdot \frac{\partial f}{\partial \mathbf{x}}(t^n + s) \right) ds. \quad (9)$$

To deal with the remaining nonlinear stiff term  $\nu f^t$  in the integral, a simple linear approximation is used:

$$f^t(t + s) = f^t(t) + \frac{s}{\Delta t} (f^t(t + \Delta t) - f^t(t)) + O(s^2). \quad (10)$$

This leads to a Crank-Nicolson-type scheme and preserves the second-order accuracy.

To build a finite volume solver, as commonly chosen for DVM-based methods in order to benefit from the conservation properties and properly handle discontinuities, the equation is then integrated on a control volume  $V_j$  centered on point  $\mathbf{x}_j$ . Therefore, in the following, we use the notations

$$f_n = \int_{V_j} f(\mathbf{x}, \mathbf{v}, t^n) d\mathbf{x} \quad \text{and} \quad (11)$$

$$F_{n+1/2} = \int_{V_j} \mathbf{v} \cdot \frac{\partial f}{\partial \mathbf{x}}(\mathbf{x}, \mathbf{v}, t^n + \frac{\Delta t}{2}) d\mathbf{x}. \quad (12)$$

With (10) and using a midpoint rule for the time integration of the flux, Eq. (9) becomes

$$\begin{aligned} f_{n+1} &= f_n e^{-v\Delta t} + e^{-v\Delta t} \left[ f_n^t \left( \frac{e^{v\Delta t}}{v\Delta t} - 1 - \frac{1}{v\Delta t} \right) \right. \\ &\quad \left. + f_{n+1}^t \left( e^{v\Delta t} + \frac{1}{v\Delta t} - \frac{e^{v\Delta t}}{v\Delta t} \right) \right] - \gamma \Delta t F_{n+1/2} \\ &= f_n e^{-v\Delta t} - \gamma \Delta t F_{n+1/2} \\ &\quad + \left( 1 - e^{-v\Delta t} \right) \times (A f_n^t + B f_{n+1}^t), \end{aligned} \quad (13)$$

where

$$\gamma = \frac{1 - e^{-v\Delta t}}{v\Delta t} \quad (14)$$

$$A = \frac{1}{v\Delta t} - \frac{e^{-v\Delta t}}{1 - e^{-v\Delta t}} \quad (15)$$

$$\text{and } B = \frac{1}{1 - e^{-v\Delta t}} - \frac{1}{v\Delta t}. \quad (16)$$

Next, in a similar way as in DUGKS<sup>2</sup>, two modified distributions can be introduced :

$$\hat{f} = \frac{1}{\gamma} \left( f e^{-v\Delta t} + (1 - e^{-v\Delta t}) A f^t \right) \quad (17)$$

$$\text{and } \tilde{f} = \frac{1}{\gamma} \left( f - (1 - e^{-v\Delta t}) B f^t \right). \quad (18)$$

Using these notations and dividing (13) by  $\gamma$  then results in a simple scheme where the advection and relaxation processes actually remain coupled in a second-order accurate time integration:

$$\tilde{f}_{n+1} = \hat{f}_n - \Delta t F_{n+1/2}. \quad (19)$$

Thus, the implicit part of the BGK operator can be handled by tracking the new distribution function  $\tilde{f}$ . And by combining (17) and (18),  $\hat{f}$  can be constructed from  $\tilde{f}$  for the next time step:

$$\hat{f} = e^{-v\Delta t} \tilde{f} + (1 - e^{-v\Delta t}) f^t. \quad (20)$$

In this equation, both pre-factors are always positive, in the interval  $[0; 1]$  and sum up to 1. The target distribution  $f^t$  can be obtained at every time step using the macroscopic moments of

$f$ , which directly correspond to those of  $\tilde{f}$  (see Section III B). The original distribution function can then easily be obtained by

$$\begin{aligned} f &= \gamma \tilde{f} + (1 - e^{-v\Delta t}) B f^t \\ &= \gamma \tilde{f} + (1 - \gamma) f^t. \end{aligned} \quad (21)$$

Note that, here as well, both pre-factors are always in  $[0; 1]$  and sum up to 1 because  $v\Delta t$  is obviously positive.

#### D. Flux evaluation

The remaining critical part is the evaluation of the flux  $F_{n+1/2}$ , for which the value of the distribution on the interfaces between mesh cells at time  $t_n + \Delta t/2$  is needed. The BGK equation is therefore integrated again with exponential differencing, but this time along a characteristic line that ends at a point  $\mathbf{x}_b$  on the cell interface to finally reconstruct  $f_{n+1/2}(\mathbf{x}_b)$  and thus calculate the flux. Along this line ( $\mathbf{x}_b + \mathbf{v}t$ ), the equation becomes simply

$$\frac{\partial f}{\partial t} = v(f^t - f). \quad (22)$$

Using modified distribution functions again to integrate within a half time step, this results in

$$\tilde{f}^r \left( \mathbf{x}_b, \mathbf{v}, t_n + \frac{\Delta t}{2} \right) = \hat{f}^r \left( \mathbf{x}_b - \mathbf{v} \frac{\Delta t}{2}, \mathbf{v}, t_n \right) \quad (23)$$

with

$$\hat{f}^r = \frac{1}{\gamma^r} \left( f e^{-v\frac{\Delta t}{2}} + (1 - e^{-v\frac{\Delta t}{2}}) A^r f^t \right) \quad (24)$$

$$\text{and } \tilde{f}^r = \frac{1}{\gamma^r} \left( f - (1 - e^{-v\frac{\Delta t}{2}}) B^r f^t \right) \quad (25)$$

where

$$\gamma^r = \frac{1 - e^{-v\frac{\Delta t}{2}}}{v\frac{\Delta t}{2}} \quad (26)$$

$$A^r = \frac{1}{v\frac{\Delta t}{2}} - \frac{e^{-v\frac{\Delta t}{2}}}{1 - e^{-v\frac{\Delta t}{2}}} \quad (27)$$

$$\text{and } B^r = \frac{1}{1 - e^{-v\frac{\Delta t}{2}}} - \frac{1}{v\frac{\Delta t}{2}}. \quad (28)$$

$\hat{f}^r$  is obtained directly from  $\tilde{f}$  by combining equations (24) and (21):

$$\hat{f}^r = \frac{\gamma}{\gamma^r} e^{-v\frac{\Delta t}{2}} \tilde{f} + \left( 1 - \frac{\gamma}{\gamma^r} e^{-v\frac{\Delta t}{2}} \right) f^t. \quad (29)$$

$\hat{f}^r$  then needs to be reconstructed from its value at the cell center to the point  $\mathbf{x}_b - \mathbf{v}\frac{\Delta t}{2}$  with a linear approximation, this time to preserve the second-order spatial accuracy:

$$\begin{aligned} \hat{f}^r \left( \mathbf{x}_b - \mathbf{v} \frac{\Delta t}{2}, \mathbf{v}, t_n \right) &= \hat{f}^r(\mathbf{x}_j, \mathbf{v}, t_n) \\ &\quad + \left( \mathbf{x}_b - \mathbf{v} \frac{\Delta t}{2} - \mathbf{x}_j \right) \nabla \hat{f}^r(\mathbf{x}_j, \mathbf{v}, t_n), \end{aligned} \quad (30)$$

where  $\mathbf{x}_j$  is the center of the cell adjacent to the the interface, chosen so that  $\mathbf{v} \cdot (\mathbf{x}_b - \mathbf{x}_j) > 0$ .

The gradients  $\nabla \hat{f}^r$  are calculated from cell-averaged values using a numerical limiter  $\phi$ , for example in 1D:

$$\nabla \hat{f}^r(\mathbf{x}_j, \mathbf{v}, t_n) = \phi \left( \frac{\hat{f}^r(\mathbf{x}_j, \mathbf{v}, t_n) - \hat{f}^r(\mathbf{x}_{j-1}, \mathbf{v}, t_n)}{\mathbf{x}_j - \mathbf{x}_{j-1}}, \frac{\hat{f}^r(\mathbf{x}_{j+1}, \mathbf{v}, t_n) - \hat{f}^r(\mathbf{x}_j, \mathbf{v}, t_n)}{\mathbf{x}_{j+1} - \mathbf{x}_j} \right). \quad (31)$$

To prevent numerical instabilities from appearing in shock regions, the van Leer limiter<sup>26</sup> can be chosen, but if not stated otherwise, a simple averaging  $\phi(a, b) = \frac{a+b}{2}$  will be used. For 2D meshes, the gradients are computed from the values in neighbouring cells with the least square approach used in Zhu, Guo, and Xu<sup>27</sup>.

Using a Stokes formula, the numerical flux is then computed for each cell  $V_j$  by summing up contributions from the interfaces  $b_k$  with area  $S_k$  and normal vector  $\mathbf{n}_k$ :

$$\begin{aligned} F_{n+1/2} &= \sum_{b_k \in \partial V_j} (\mathbf{n}_k \cdot \mathbf{v}) f(\mathbf{x}_b, \mathbf{v}, t_n + \frac{\Delta t}{2}) S_k \\ &= \sum_{b_k \in \partial V_j} (\mathbf{n}_k \cdot \mathbf{v}) \left( \gamma^r \tilde{f}^r \left( \mathbf{x}_b, \mathbf{v}, t_n + \frac{\Delta t}{2} \right) + (1 - \gamma^r) f_{n+1/2}^t(\mathbf{v}) \right) S_k, \end{aligned} \quad (32)$$

where  $f_{n+1/2}^t$  is constructed from the moments of  $\tilde{f}^r(\mathbf{x}_b, \cdot, t_n + \frac{\Delta t}{2})$ .

### E. Properties of the scheme

As ED-DVM does not rely on a splitting of the advection and relaxation processes, the mean free path of the particles do not need to be resolved, allowing for much larger mesh cells than those required for DSMC simulations in near-continuum cases. The second-order convergence, proved analytically for the temporal dimension in Appendix A, also improves accuracy compared to the particle-based methods, usually only reaching a maximum convergence order of 1. Besides, the implicit integration of the relaxation term allows for the time step to be chosen larger than the relaxation time. However, due to the overall explicit nature of the method, the Courant-Friedrichs-Lewy (CFL) condition still needs to be fulfilled.

The devised ED-DVM is in fact an asymptotic preserving method, therefore able to solve the BGK equation in all regimes with second-order accuracy in both time and space. Indeed, in the free molecular flow limit ( $\frac{1}{v} = \tau \gg \Delta t$ ), all rescaled distribution functions are equivalent to the original  $f$  and the scheme then solves a simple advection equation for each velocity point, retaining second-order finite volumes discretization. Besides, in the continuum limit ( $\tau \ll \Delta t$ ), it can be shown that the time-dependent Chapman-Enskog Navier-Stokes distribution function is retrieved at the cell boundaries

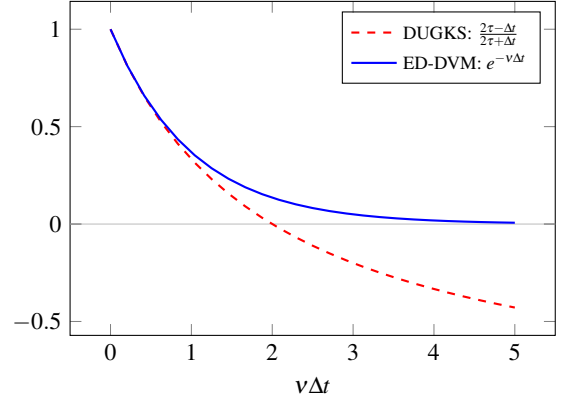


FIG. 1: Pre-factor in front of  $\tilde{f}$  in the equation to build  $\hat{f}$ .

for the flux calculation:

$$\begin{aligned} f(\mathbf{x}_b, \mathbf{v}, t_{n+1/2}) &= f^t(\mathbf{x}_b, \mathbf{v}, t_n) - \tau D_t f^t(\mathbf{x}_b, \mathbf{v}, t_n) \\ &\quad + \frac{\Delta t}{2} \partial_t f^t(\mathbf{x}_b, \mathbf{v}, t_n) + O(\text{Kn}^2). \end{aligned} \quad (33)$$

The proof of the asymptotic behavior of the method can be found with more details in Appendix B.

Furthermore, the conservative property of the BGK operator and the use of a finite volume scheme ensure that density, momentum, and energy are conserved up to the numerical error introduced by the velocity discretization. Indeed, the discretized collision operator is not conservative but properly choosing the velocity quadrature reduces the induced numerical deviation, which has therefore not been a problem in the following simulations. A fully conservative scheme could be implemented following the idea of Mieussens<sup>4</sup>, but this would come with the additional cost of solving a system of at least 5 nonlinear equations at every time step.

The main difference between ED-DVM and DUGKS is the aforementioned positivity of the pre-factors used in the "rescaling" that combines linearly the distribution function  $f$  with the target  $f^t$ . This property, in addition to ensuring the positivity of the distribution function as long as the target is also positive, is what allows the direct extension of this DVM to a stochastic particle scheme. The factors regarded as probabilities in such a method<sup>1</sup> would mainly be those in Eq. (20) and they indeed remain between 0 and 1 independently of the relaxation frequency and time step, which is not the case with their DUGKS equivalents, as displayed on Fig. 1.

## III. NUMERICAL IMPLEMENTATION

### A. Discrete velocity quadratures

Focusing now on the velocity discretization, the choice of the quadrature points and weights depends on the problem considered. The commonly used discretizations are based either on the Gauss-Hermite quadrature or on composite Newton-Cotes rules<sup>2,28,29</sup>. The quadrature rules are given here in one dimension but can be simply extended to two or three

dimensions by discretizing the additional velocity directions in the same manner and multiplying the respective weights.

For flows that can be considered almost isothermal (around a reference temperature  $T_{GH}$ ) and with no region where the particle distribution is too far from thermal equilibrium, a Gauss-Hermite quadrature can be used. With  $h_{N,i}$  the  $N$  roots of the Hermite polynomial  $H_N$ , the velocity discretization points and weights are

$$v_i = \sqrt{2RT_{GH}}h_{N,i}, \quad w_i = \sqrt{2RT_{GH}} \frac{2^{N-1}N!\sqrt{\pi}}{N^2[H_{N-1}(h_{N,i})]^2} e^{h_{N,i}^2}. \quad (34)$$

This choice of quadrature allows for an accurate representation of distribution functions with a limited number of points, provided that the deviation from equilibrium is small, and ensures that the BGK relaxation operator is conservative in the purely isothermal case<sup>14</sup>. The precision of this quadrature can be improved by increasing the polynomial degree  $N$  and therefore the number of velocity points.

In cases where strong non-equilibrium effects should be observed (e.g. shocks, hypersonic or highly rarefied flows), a uniform choice of discretization, without assuming a Gaussian shape for the distribution, is preferable. A Newton-Cotes quadrature is therefore used to discretize the velocity space for such simulations, spanning a range  $[v_{min}, v_{max}]$  with evenly spaced points. Concerning the quadrature weights, since high order Newton-Cotes formulas do not necessarily increase the interpolation accuracy, we divide  $[v_{min}, v_{max}]$  into smaller equal intervals in which low order formulas are used, while ensuring that this results in an  $N$  point composite quadrature.

## B. Calculation of the moments

In order to reduce the computational cost when simulating a  $d$ -dimensional problem with  $d \leq 2$ , reduced distribution functions are introduced, as commonly done<sup>28,30</sup> to avoid discretizing the velocity space in the unnecessary directions:

$$g(\mathbf{x}, \mathbf{v}', t) = \int f(\mathbf{x}, \mathbf{v}', \boldsymbol{\eta}, t) d\boldsymbol{\eta} \quad (35)$$

$$\text{and } h(\mathbf{x}, \mathbf{v}', t) = \int \boldsymbol{\eta}^2 f(\mathbf{x}, \mathbf{v}', \boldsymbol{\eta}, t) d\boldsymbol{\eta} \quad (36)$$

where, setting the  $x, y$  and  $z$  velocity components as  $\mathbf{v} = (\xi_1, \xi_2, \xi_3)^T$ , we write  $\mathbf{v}' = (\xi_1, \dots, \xi_d)^T$  and  $\boldsymbol{\eta} = (\xi_{d+1}, \dots, \xi_3)^T$ . For the Shakhov model, the corresponding target distributions are then:

$$\begin{aligned} g^S(\mathbf{v}') &= \int f^S(\mathbf{v}) d\boldsymbol{\eta} \\ &= g^M \left[ 1 + (1 - \text{Pr}) \frac{\mathbf{c}' \cdot \mathbf{q}}{5\rho(RT)^2} \left( \frac{\mathbf{c}'^2}{RT} - d - 2 \right) \right] \quad (37) \\ h^S(\mathbf{v}') &= \int \boldsymbol{\eta}^2 f^S(\mathbf{v}) d\boldsymbol{\eta} \\ &= g^M (3 - d) RT \\ &\quad \times \left[ 1 + (1 - \text{Pr}) \frac{\mathbf{c}' \cdot \mathbf{q}}{5\rho(RT)^2} \left( \frac{\mathbf{c}'^2}{RT} - d \right) \right] \quad (38) \end{aligned}$$

with  $g^M = \frac{\rho}{(2\pi RT)^{d/2}} e^{-\frac{\mathbf{c}'^2}{2RT}}$  and  $\mathbf{c}' = \mathbf{v}' - \mathbf{u}$ .

The evolution of these reduced distributions is also obtained from the BGK equation by simply replacing  $f$  with  $g$  or  $h$ , and  $f^S$  with  $g^S$  or  $h^S$ . Therefore, the whole scheme detailed above is applied simultaneously to  $g$  and  $h$ , and the moments used to construct the target distributions  $g^S$  and  $h^S$  are directly computed through discrete sums:

$$\mathbf{W} = \begin{pmatrix} \rho \\ \rho \mathbf{u} \\ \rho E \end{pmatrix} = \sum_{i=1}^N w_i \left[ \boldsymbol{\psi}(\mathbf{v}'_i) \tilde{g}(\mathbf{x}, \mathbf{v}'_i, t) + \boldsymbol{\zeta} \tilde{h}(\mathbf{x}, \mathbf{v}'_i, t) \right] \quad (39)$$

with  $\boldsymbol{\zeta} = (0, 0, 1)^T$  and  $\boldsymbol{\psi} = (1, \mathbf{v}, \mathbf{v}^2/2)^T$ .

The heat flux vector needs to be rescaled according to the exponential differencing<sup>1</sup> using (21):

$$\mathbf{q} = \frac{1 - e^{-v\Delta t \text{Pr}}}{v\Delta t \text{Pr}} \tilde{\mathbf{q}} \quad (40)$$

$$\text{with } \tilde{\mathbf{q}} = \frac{1}{2} \sum_{i=1}^N w_i \mathbf{c}'_i \left[ \mathbf{c}'_i^2 \tilde{g}(\mathbf{x}, \mathbf{v}'_i, t) + \tilde{h}(\mathbf{x}, \mathbf{v}'_i, t) \right]. \quad (41)$$

## C. Boundary conditions

Two types of boundary conditions have been implemented in this study for gas/wall interactions: specular and diffusive reflection. In both cases, the first step is the construction of a boundary-specific distribution function on the wall. In order to validate these boundary conditions, a single one is applied at each wall in the following test cases, but for more realistic wall interactions, a linear combination of the specular and diffusive wall distributions could be used.

The specular reflection distribution is the same as the inner cell distribution, but obtained after perfectly reflecting the velocities directed onto the wall:

$$\begin{aligned} \forall \mathbf{v} \text{ so that } \mathbf{v} \cdot \mathbf{n}_w < 0, \\ f(\mathbf{x}_w, \mathbf{v}, t) &= f(\mathbf{x}_w, \mathbf{v} - 2(\mathbf{v} \cdot \mathbf{n}_w) \mathbf{n}_w, t). \quad (42) \end{aligned}$$

This boundary condition is only applicable to a static wall with a normal vector  $\mathbf{n}_w$  aligned with the velocity grid, so that for a grid point  $\mathbf{v}_i$ , the velocity  $\mathbf{v}_i - 2(\mathbf{v}_i \cdot \mathbf{n}_w) \mathbf{n}_w$  is another grid point. If more complex geometries have to be simulated with this type of boundaries, a velocity interpolation could be used<sup>31</sup>.

The diffusive reflection distribution is a simple Maxwellian  $f_w^M$  with wall temperature and velocity, first calculated with arbitrary density  $\rho_{\text{tmp}}$ . The actual wall density is then adjusted to conserve the number of particles hitting the wall<sup>32</sup>:

$$\rho_w = -\rho_{\text{tmp}} \times \left[ \sum_{\mathbf{v} \cdot \mathbf{n} > 0} (\mathbf{v} \cdot \mathbf{n}) f_w^M \right]^{-1} \times \sum_{\mathbf{v} \cdot \mathbf{n} < 0} (\mathbf{v} \cdot \mathbf{n}) f(\mathbf{x}_w, \mathbf{v}, t). \quad (43)$$

In order to preserve the second-order accuracy at the boundaries, ghost cells are created outside of the domain to be able to compute gradients and perform the reconstruction step in the boundary cells. In these ghost cells, the value of the

distribution function is interpolated from inner and wall values while ensuring compatibility with the reconstruction algorithm, following the method described in Baranger *et al.*<sup>33</sup>. The finite volume flux can then be calculated as inside of the domain.

#### D. Algorithm

The resulting exponential differencing DVM (ED-DVM) algorithm consists of updating the distribution function  $\tilde{f}_n$  in every mesh cell at each time step. This procedure, implemented in the PIC-DSMC code PICLas<sup>34</sup>, can be summarized as follows:

1. Compute the target distribution  $f_n^t$  using the macroscopic values obtained via the moments of  $\tilde{f}_n$  (Eq. 39 and 41).
2. Compute the distribution function  $\hat{f}_n^r$  from  $\tilde{f}_n$  (Eq. 29).
3. Compute the necessary distributions at the boundaries, depending on the boundary condition.
4. Compute the spatial gradients of  $\hat{f}_n^r$  (Eq. 31).
5. Reconstruct  $\tilde{f}_{n+1/2}^r$  at the cell interfaces (Eq. 30 and 23).
6. Sum up the flux contributions at interfaces and boundaries (Eq. 32).
7. Compute the distribution function  $\hat{f}_n$  from  $\tilde{f}_n$  (Eq. 20).
8. Update the distribution function to  $\tilde{f}_{n+1}$  (Eq. 19).

## IV. RESULTS

### A. Heat flux relaxation

As a first test case, a spatially homogeneous heat flux relaxation is considered, in order to validate the second-order accuracy of the ED-DVM scheme in time. A single adiabatic mesh cell is filled with argon gas at density  $\rho = 1.79 \text{ kg/m}^3$  and temperature  $T = 273 \text{ K}$ . Only one velocity direction is allowed and the heat flux is initially set in that direction to  $q_x(0) = \rho(3RT)^{3/2}$  using Grad's 13 moments distribution<sup>18</sup> with a pressure tensor equal to zero:

$$f_{init} = f^M \left[ 1 - \frac{\mathbf{q} \cdot \mathbf{c}}{\rho R^2 T^2} \left( 1 - \frac{\mathbf{c}^2}{5RT} \right) \right]. \quad (44)$$

The heat flux then relaxes exponentially towards equilibrium at a rate  $\tau = 1/v$ . Fig. 2a shows that ED-DVM is able to properly resolve this test case even with time steps several times larger than the relaxation time. Furthermore, the error comparison (Fig. 2b) clearly displays the expected second-order convergence in time, with ED-DVM performing even slightly better than DUGKS at large time steps.

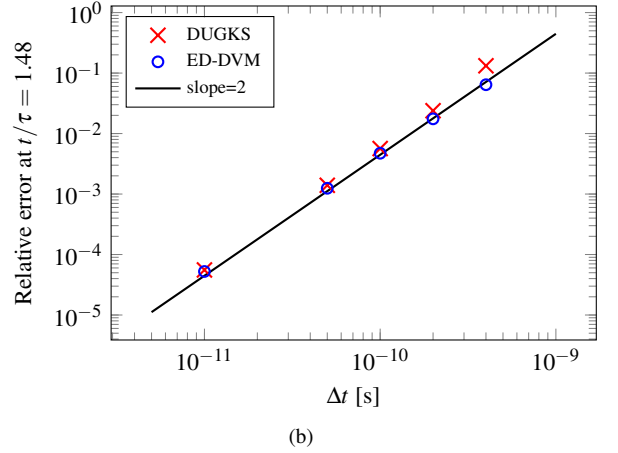
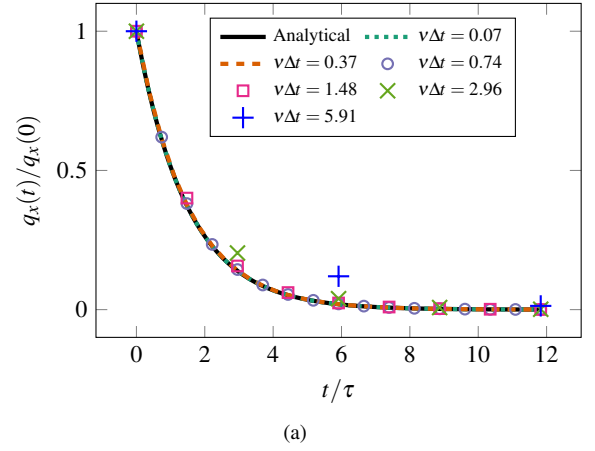
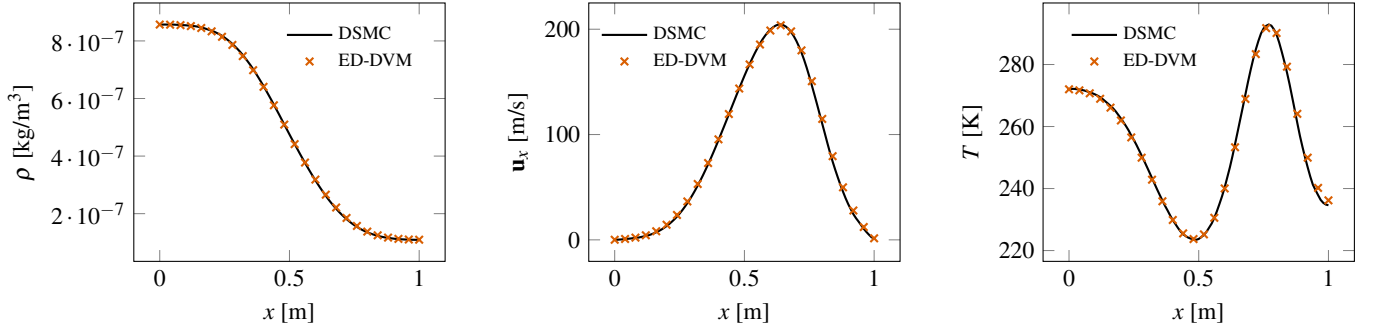
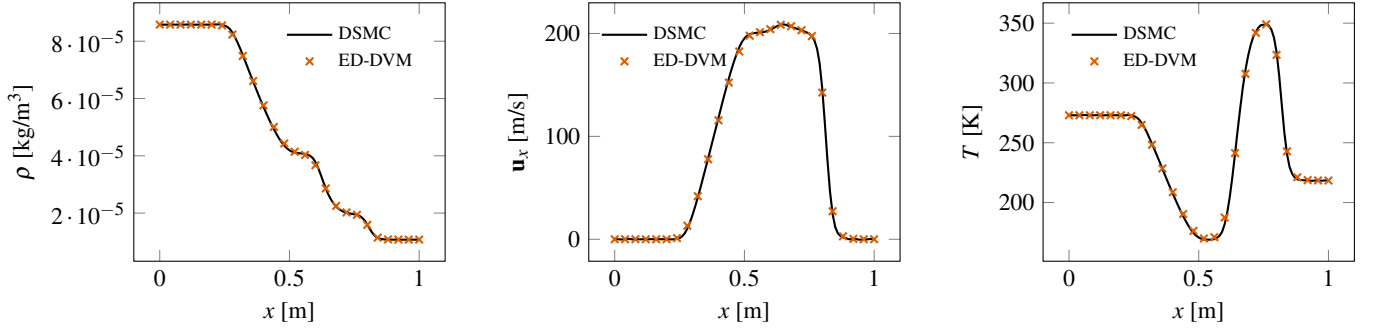


FIG. 2: Heat flux relaxation with different time step sizes  $\Delta t$ : (a) ED-DVM results, (b) Error convergence for ED-DVM and DUGKS

### B. Sod shock tube

The second test case is the widely studied Sod shock tube problem, where a 1D tube of length 1 m contains a fluid, here argon, with an initial discontinuity in density and temperature at  $x = 0.5 \text{ m}$ . The left and right temperatures are set to  $T_l = 273 \text{ K}$  and  $T_r = 218.4 \text{ K}$  while the initial density is chosen depending on the flow's Knudsen number, with the condition  $\rho_r = 0.125\rho_l$ .

The tube was discretized in 100 equal cells and two different regimes were investigated: a rarefied case with a Knudsen number of  $\text{Kn} = 0.1$  and a denser regime with  $\text{Kn} = 0.001$ . To solve both cases with ED-DVM and in order to respect the CFL condition with a CFL number of  $\frac{\max(|v_{min}|, |v_{max}|)\Delta t}{\Delta x} = 0.9$ , the time step is set to  $\Delta t = 6.667 \times 10^{-6} \text{ s}$  and the uniform velocity space limited to  $[-4\sqrt{2RT_l}; 4\sqrt{2RT_l}]$ . The van Leer limiter was used in order to avoid any nonphysical oscillations due to the high gradients around  $x = 0.5 \text{ m}$ . The shock then propagates for  $7 \times 10^{-4} \text{ s}$  and results for the first three moments are compared at that point in time to those obtained via Discrete Simulation Monte-Carlo (DSMC).

FIG. 3: Sod shock tube at  $\text{Kn} = 0.1$ FIG. 4: Sod shock tube at  $\text{Kn} = 0.001$ 

The Variable Hard Sphere collision model was used for the DSMC reference simulations in order to match the definition of viscosity in the BGK equation. In the low density case, the DSMC reference results could be obtained with the same time step but in the near-continuum case, a 20 times smaller time step and adaptive subcells had to be used in order to resolve the mean collision time and the mean free path. Furthermore, the need of around  $10^6$  particles per cell to reduce the stochastic noise induced by DSMC greatly exceeded the computational cost of ED-DVM on this unsteady flow that prevents any time averaging. Indeed, only 50 velocity points were needed in the rarefied case to match DSMC (Fig. 3), while 15 were enough to reach good accuracy in the dense regime (Fig. 4).

Table I compares in more details the CPU time needed using the parallelized code PICLas, already heavily optimized for DSMC. The time required by ED-DVM is so short that most of the cost comes from the code initialization and the influence of the velocity grid size is negligible. Besides, as the acceptable level of noise in the DSMC results is a rather arbitrary choice, the number of simulation particles was here fixed so as to resolve the mean free path in the dense case. The times displayed for DSMC are therefore obtained using only 300 particles per cell in the left part of the domain (the noise-free DSMC simulations used for validation lasted about 8 hours in the dense case). This however resulted in a stochastic noise level leading to an error on the macroscopic variables of around 10%.

TABLE I: Time needed to solve the Sod shock tube problem on 10 cores of an AMD EPYC 7713 processor.

$\text{Kn}$	DSMC	ED-DVM
0.001	4.59 s	0.06 s
0.1	0.68 s	0.09 s

### C. Force-driven Poiseuille flow

In order to examine more in depth the spatio-temporal convergence of the ED-DVM, a force-driven Poiseuille flow was simulated at two different Knudsen numbers using various space and time resolutions. This test case consists in a one dimensional domain with a length of  $L_y = 1$  m, where an argon flow is accelerated by a constant force  $F_x$  perpendicular to the domain, chosen here so that  $\frac{\rho}{m}F_x = 10^{-2}$  Pa/m, where  $m$  is the molecular mass. This force is applied in two steps, adding half the force before and after every time step, resulting in a Strang splitting approach, as suggested in Wang *et al.*<sup>29</sup>. An equilibrium approximation is made here, so that each half force term can be simply added to the distribution function via:

$$f_{new} = f_{old} + \frac{\Delta t}{2} \frac{F_x}{m} \frac{\partial f}{\partial v_x} \approx f_{old} + \frac{\Delta t}{2} \frac{F_x c_x}{mRT} f^M. \quad (45)$$

Up to a Knudsen number of 0.1, this approximation yields accurate results, but for more rarefied flows, the term  $\frac{\partial f}{\partial v_x}$  is cal-

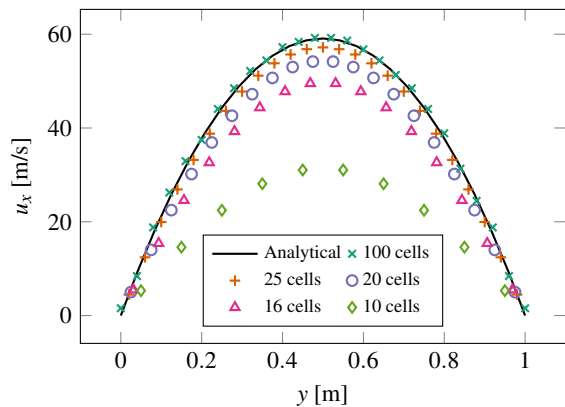


FIG. 5: Poiseuille flow at  $Kn=0.001$ : velocity profile obtained with ED-DVM using different resolutions.

culated using centered finite differences in the velocity space. The boundaries at  $y=0$  m and  $y=1$  m are immobile and diffusive, with a wall temperature equal to the initial gas temperature  $T_0=273$  K.

This Poiseuille flow is first simulated in near-continuum conditions, with  $Kn=0.001$ , using a  $5 \times 5$  points Gauss-Hermite quadrature with reference temperature  $T_{GH}=T_0$ . The CFL number is fixed to 0.9 while the time step and spatial resolution are changed proportionally. The resulting velocity profiles are compared on Fig. 5 to the continuum analytical solution<sup>35</sup>:

$$u_x = \frac{\rho F_x}{m} \frac{L_y y - y^2}{2\mu}. \quad (46)$$

Very good agreement was obtained with the 100 cells mesh, where the relaxation factor is around  $v\Delta t=3$ , with even acceptable accuracy with 25 cells and a relaxation factor as high as 12.

A more rarefied case at  $Kn=0.1$  is also simulated, and compared to a reference DSMC simulation on Fig. 6. Regarding the velocity discretization, no substantial improvement in accuracy was obtained beyond  $101 \times 101$  equally spaced points between  $-3000$  and  $3000$  m/s, so all ED-DVM simulations were performed with this quadrature. In this case, the low relaxation frequency combined to the CFL condition prevented us from investigating high relaxation factors, but with a CFL number of 0.9, a simple 10 cells mesh proved enough to accurately match the DSMC results. It should however be noted that the Shakhov model cannot retrieve the high order super-Burnett terms, which are necessary to produce the specific temperature and higher moments profiles at high Knudsen numbers for this flow<sup>36</sup>. Nevertheless, our method was sufficient in this case when focusing only the velocity profile. As both DSMC and ED-DVM are explicit time-accurate methods, the steady state was reached at the same point in simulation time, but the DSMC solution is obtained by letting the simulation run after reaching that steady state, and averaging over time until statistical noise is reduced to reasonable levels.

Furthermore, this analysis with varying spatio-temporal

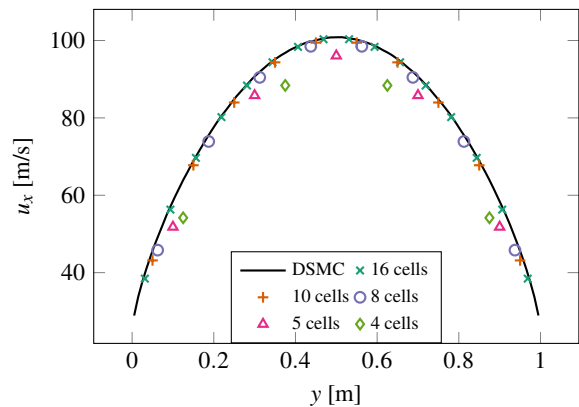


FIG. 6: Poiseuille flow at  $Kn=0.1$ : velocity profile obtained with ED-DVM using different resolutions.

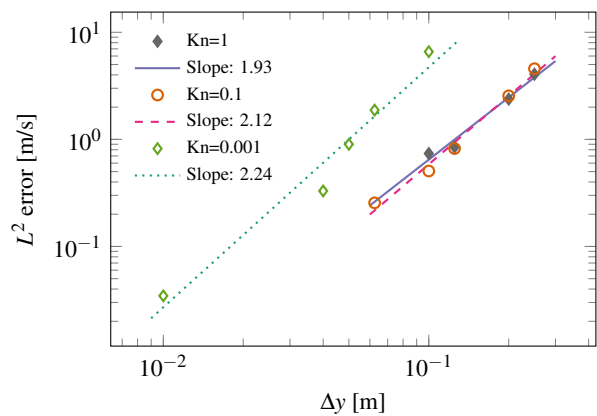


FIG. 7: Poiseuille flow: error convergence of the velocity  $u_x$  in the dense and rarefied cases.

discretization allows the error convergence in these cases to be shown on Fig. 7. A third regime, with  $Kn=1$ , has also been simulated, but the non-equilibrium effects are then too important for the Shakhov-BGK model to give the same velocity profile as DSMC. It is therefore only shown in this comparison, computing the error to a highly resolved ED-DVM solution, purely for the sake of convergence analysis. It is then clear that the ED-DVM is second-order accurate in space and time, regardless of the rarefaction level.

#### D. Lid-driven cavity flow

The lid-driven cavity flow was then simulated to observe the method's performance on a well-studied fully 2D case, with reference results available for a wide range of Reynolds numbers, obtained with Navier-Stokes solvers<sup>37</sup> or discrete velocity methods<sup>2,7</sup>. Using a particle-based method to simulate this low Mach number flow would be much less efficient due to the particularly high number of particles needed to reach a reasonable signal-to-noise ratio. Indeed, this test case consists of a square cavity with diffusive boundaries where the flow of the

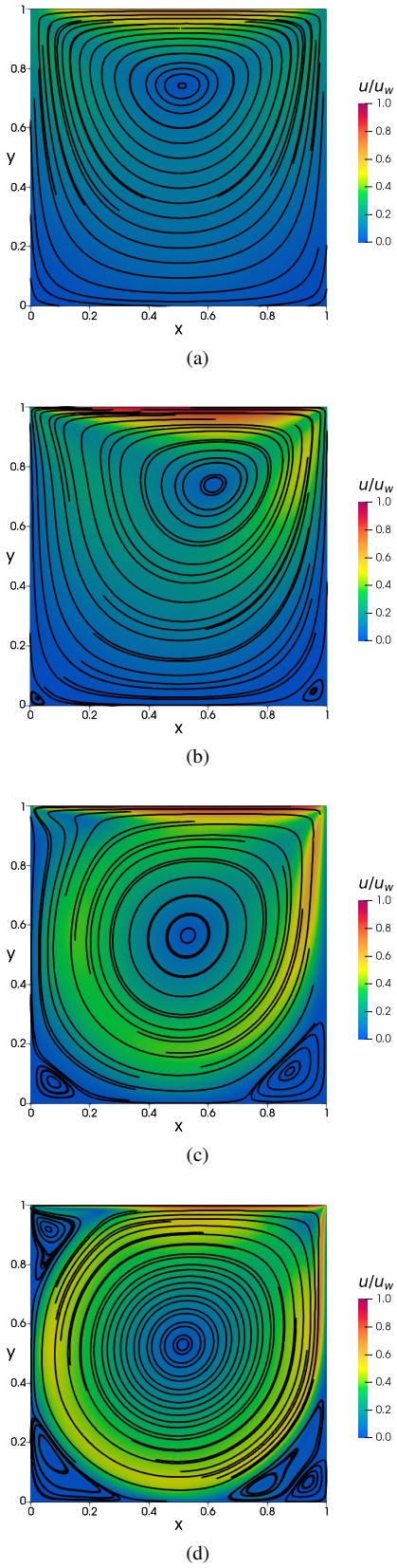


FIG. 8: Lid-driven cavity flow: velocity field lines and magnitude, simulated with ED-DVM. (a)  $Kn = 0.075$ , (b)  $Re = 100$ , (c)  $Re = 1000$ , (d)  $Re = 10,000$

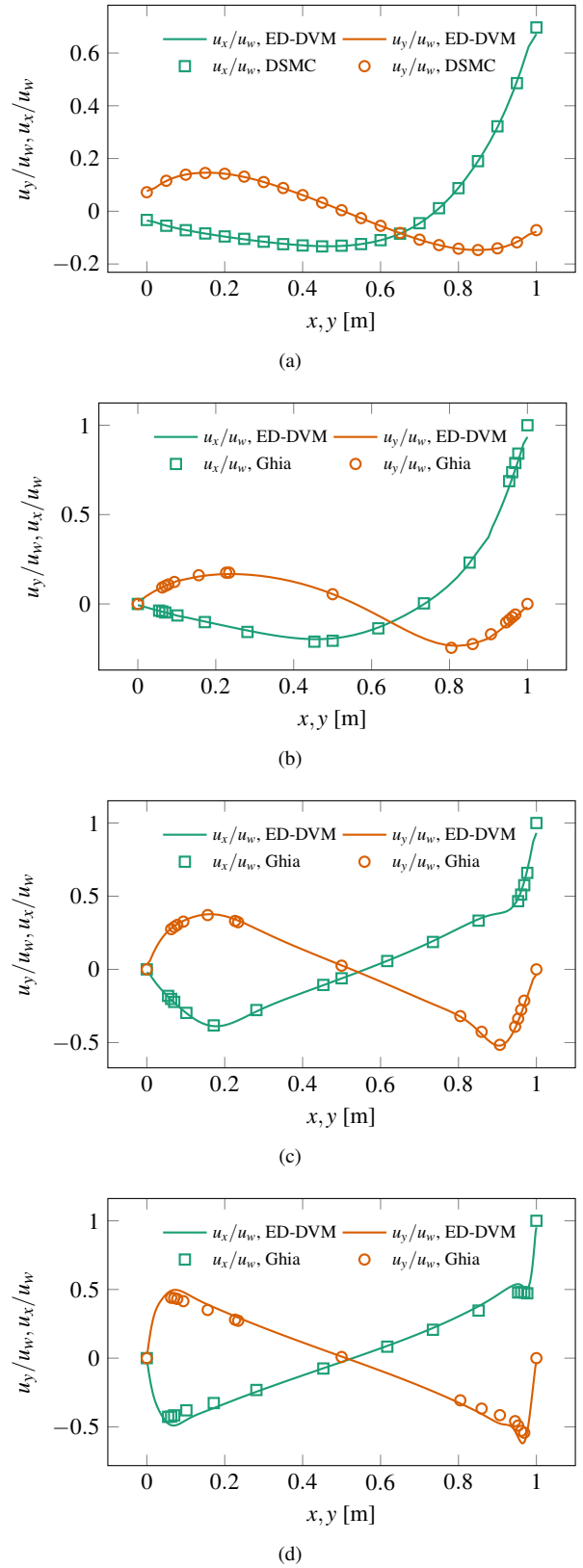


FIG. 9: Lid-driven cavity flow:  $x$ -velocity along a central vertical line (green) and  $y$ -velocity along a central horizontal line (orange). (a)  $Kn = 0.075$ , (b)  $Re = 100$ , (c)  $Re = 1000$ , (d)  $Re = 10,000$

initially motionless gas is only driven by the top wall moving at a constant slow velocity  $u_w$  in its own plane. The initial and wall temperatures are set to  $T_0 = T_w = 273$  K while we use the same lid velocity  $u_w = 50$  m/s in all cases, changing the argon density (and therefore the kinematic viscosity) to obtain the desired Reynolds number.

The mesh grid was adapted depending on the Reynolds number in order to resolve the arising secondary vortices, which can be seen on Fig. 8.  $50 \times 50$  cells were used for  $Re = 100$ ,  $100 \times 100$  for  $Re = 1000$  and  $200 \times 200$  for  $Re = 10,000$ , all grids being non uniform with higher resolution in vortex regions. A  $5 \times 5$  Gauss-Hermite velocity grid was sufficient in all cases as the most rarefied case studied here only has a Knudsen number of 0.002 and the low-speed nature of the flow limits the non-equilibrium effects. The CFL number of 0.9 was sufficient to match the reference results of Ghia, Ghia, and Shin<sup>37</sup> obtained with a Navier-Stokes solver.

A more rarefied simulation at  $Kn = 0.075$  was also carried out, using a  $50 \times 50$  uniform mesh, a  $28 \times 28$  Gauss-Hermite velocity grid and a CFL number of 0.9. As the Navier-Stokes equations do not give accurate results in this regime<sup>38</sup>, a highly resolved DSMC simulation was used as the reference in this case.

Comparisons to the references are shown on Fig. 9 where the values of the velocity components  $u_x$  and  $u_y$  are taken along a line perpendicular to the direction of the component and passing through the center of the cavity. The ED-DVM was able to accurately capture the features of this flow even for the high Reynolds number of 10,000 where sharp variations in the velocity field arise.

## V. CONCLUSION

A second-order asymptotic preserving BGK solver was presented and evaluated on various test cases and in different regimes. Although the performances are similar to pre-existing DVM schemes such as DUGKS, the main advantage of ED-DVM is that all operations on distribution functions ensure the positivity of every term. This feature, combined to the asymptotic preserving and second-order properties reached without introducing implicit steps in the final algorithm, allows for a straightforward correspondence between high accuracy deterministic and stochastic schemes.

While the ED-DVM has the usual advantages inherent to DVMs compared to particle solvers when it comes to low-velocity near-continuum flows, its particle adaptation presented in Pfeiffer, Garmirian, and Gorji<sup>1</sup> can become more efficient in rarefied and high-speed regimes. In order to fully benefit from the efficiency of the exponential differencing approach, a coupling between the two solvers, either in velocity or physical space, would be valuable as future development. Besides, the ED-DVM could be extended to simulate molecular gases or more costly cases with better optimized velocity grids.

## ACKNOWLEDGMENTS

This project has received funding from the European Research Council (ERC) under the European Union's Horizon 2020 research and innovation programme (grant agreement No. 899981 MEDUSA).

The authors also thank the High Performance Computing Center Stuttgart (HLRS) for granting the computational time that has allowed the execution of the presented simulations.

## Appendix A: Temporal convergence analysis

The second-order temporal accuracy of ED-DVM can be easily demonstrated when assuming a Maxwellian target distribution and homogeneity of the solution in space. The temporal change is then defined by:

$$\frac{df}{dt} = \mathbf{v}(f^M - f). \quad (\text{A1})$$

The Taylor expansion of  $f(t+h) = f_{t+h}$  gives:

$$\begin{aligned} f_{t+h} &= f_t + h \frac{df}{dt} + \frac{h^2}{2} \frac{d^2f}{dt^2} + O(h^3) \\ &= f_t + h\mathbf{v}(f^M - f_t) - \frac{(h\mathbf{v})^2}{2}(f^M - f_t) + O(h^3) \end{aligned} \quad (\text{A2})$$

since

$$\frac{d^2f}{dt^2} = -\mathbf{v} \frac{df}{dt} \quad (\text{A3})$$

in this homogeneous Maxwellian case.

The homogeneity also gives  $\tilde{f} = \hat{f}$ , therefore, using ED-DVM with a time step  $\Delta t = h$ :

$$\begin{aligned} f_{t+h} &= \frac{1 - e^{-h\mathbf{v}}}{h\mathbf{v}} \left( \frac{h\mathbf{v}e^{-h\mathbf{v}}}{1 - e^{-h\mathbf{v}}} f_t + (1 - B)f^M \right) + (1 - A)f^M \\ &= e^{-h\mathbf{v}} f_t + (A - e^{-h\mathbf{v}} + 1 - A)f^M \\ &= e^{-h\mathbf{v}} f_t + (1 - e^{-h\mathbf{v}})f^M. \end{aligned} \quad (\text{A4})$$

Now, taking the Taylor expansion of the exponential function

$$e^{-h\mathbf{v}} = 1 - h\mathbf{v} + \frac{(h\mathbf{v})^2}{2} + O(h^3) \quad (\text{A5})$$

and using this into equation (A4):

$$\begin{aligned} f_{t+h} &= \left(1 - h\mathbf{v} + \frac{(h\mathbf{v})^2}{2}\right) f_t + \left(1 - 1 + h\mathbf{v} - \frac{(h\mathbf{v})^2}{2}\right) f^M \\ &= f_t + h\mathbf{v}(f^M - f_t) - \frac{(h\mathbf{v})^2}{2}(f^M - f_t) + O(h^3). \end{aligned} \quad (\text{A6})$$

This matches the expansion of equation (A2), showing that the temporal integration used in the ED-DVM is at least second-order accurate.

## Appendix B: Asymptotic analysis

In the free molecular flow limit ( $\nu\Delta t \rightarrow 0$ ), using  $e^x \sim 1 + x$  yields  $\hat{f} = \tilde{f} = f$ . ED-DVM then becomes a simple second-order finite volume scheme solving an advection equation:

$$f_{n+1} = f_n - \Delta t F_{n+1/2}. \quad (\text{B1})$$

In the continuum limit, the approach of Guo, Xu, and Wang<sup>2</sup> is followed and the distribution function is expressed by its Chapman-Enskog expansion:

$$f(t) \approx f^M(t) - \tau D_t f^M(t) + O(D_t^2) \quad (\text{B2})$$

where  $D_t = (\partial_t + \mathbf{v}\nabla)$  and using the Maxwellian as target distribution. Rewriting Eq. (25) as

$$f = \gamma^r \tilde{f}^r + (1 - \gamma^r) f^M \quad (\text{B3})$$

and using Eqs. (23) and (24), the distribution at a cell boundary becomes, with  $h = \Delta t/2$ :

$$\begin{aligned} f(\mathbf{x}_b, t+h) &= \gamma^r \hat{f}^r(\mathbf{x}_b - \mathbf{v}h, t) \\ &\quad + (1 - \gamma^r) f^M(\mathbf{x}_b, t+h) \\ &= e^{-\nu h} f(\mathbf{x}_b - \mathbf{v}h, t) \\ &\quad + (\gamma^r - e^{-\nu h}) f^M(\mathbf{x}_b - \mathbf{v}h, t) \\ &\quad + (1 - \gamma^r) f^M(\mathbf{x}_b, t+h) \\ &= e^{-\nu h} [f(\mathbf{x}_b, t) - h\mathbf{v} \cdot \nabla f(\mathbf{x}_b, t)] \\ &\quad + (\gamma^r - e^{-\nu h}) [f^M(\mathbf{x}_b, t) - h\mathbf{v} \cdot \nabla f^M(\mathbf{x}_b, t)] \\ &\quad + (1 - \gamma^r) [f^M(\mathbf{x}_b, t) + h\partial_t f^M(\mathbf{x}_b, t)] + O(h^2) \end{aligned} \quad (\text{B4})$$

The variable  $\mathbf{v}$  in the arguments of the distributions is omitted for more clarity. Using Eq. (B2) then gives:

$$\begin{aligned} f(\mathbf{x}_b, t+h) &= e^{-\nu h} [f^M(\mathbf{x}_b, t) - \tau D_t f^M(\mathbf{x}_b, t)] \\ &\quad + (\gamma^r - e^{-\nu h}) f^M(\mathbf{x}_b, t) \\ &\quad - h\mathbf{v} \cdot \left( e^{-\nu h} \nabla f^M(\mathbf{x}_b, t) + (\gamma^r - e^{-\nu h}) \nabla f^M(\mathbf{x}_b, t) \right) \\ &\quad + (1 - \gamma^r) [f^M(\mathbf{x}_b, t) + h\partial_t f^M(\mathbf{x}_b, t)] + O(h^2) + O(\partial^2) \\ &= f^M(\mathbf{x}_b, t) - \tau D_t f^M(\mathbf{x}_b, t) \\ &\quad + h\partial_t f^M(\mathbf{x}_b, t) + O(h^2) + O(\partial^2) \end{aligned} \quad (\text{B5})$$

which is in fact a Chapman-Enskog Navier-Stokes distribution.

<sup>1</sup>M. Pfeiffer, F. Garmirian, and M. H. Gorji, “Exponential Bhatnagar-Gross-Krook integrator for multiscale particle-based kinetic simulations,” *Physical Review E* **106**, 025303 (2022).

<sup>2</sup>Z. Guo, K. Xu, and R. Wang, “Discrete unified gas kinetic scheme for all Knudsen number flows: Low-speed isothermal case,” *Physical Review E* **88**, 033305 (2013).

<sup>3</sup>K. Xu and J.-C. Huang, “A unified gas-kinetic scheme for continuum and rarefied flows,” *Journal of Computational Physics* **229**, 7747–7764 (2010).

<sup>4</sup>L. Mieussens, “Discrete velocity model and implicit scheme for the bgk equation of rarefied gas dynamics,” *Mathematical Models and Methods in Applied Sciences* **10**, 1121–1149 (2000).

<sup>5</sup>M. A. Gallis and J. R. Torczynski, “Investigation of the ellipsoidal-statistical Bhatnagar-Gross-Krook kinetic model applied to gas-phase transport of heat and tangential momentum between parallel walls,” *Physics of Fluids* **23**, 030601 (2011).

<sup>6</sup>M. Pfeiffer, “Particle-based fluid dynamics: Comparison of different Bhatnagar-Gross-Krook models and the direct simulation Monte Carlo method for hypersonic flows,” *Physics of Fluids* **30**, 106106 (2018).

<sup>7</sup>F. Fei, J. Zhang, J. Li, and Z. Liu, “A unified stochastic particle Bhatnagar-Gross-Krook method for multiscale gas flows,” *Journal of Computational Physics* **400**, 108972 (2020).

<sup>8</sup>F. Fei, Y. Ma, J. Wu, and J. Zhang, “An efficient algorithm of the unified stochastic particle Bhatnagar-Gross-Krook method for the simulation of multi-scale gas flows,” *Advances in Aerodynamics* **3**, 18 (2021).

<sup>9</sup>J. Zhang, B. John, M. Pfeiffer, F. Fei, and D. Wen, “Particle-based hybrid and multiscale methods for nonequilibrium gas flows,” *Advances in Aerodynamics* **1**, 12 (2019).

<sup>10</sup>M. Pfeiffer, A. Mirza, and P. Nizenkov, “Evaluation of particle-based continuum methods for a coupling with the direct simulation Monte Carlo method based on a nozzle expansion,” *Physics of Fluids* **31**, 073601 (2019).

<sup>11</sup>M. H. Gorji and P. Jenny, “An efficient particle Fokker-Planck algorithm for rarefied gas flows,” *Journal of Computational Physics* **262**, 325–343 (2014).

<sup>12</sup>C. Liu, Y. Zhu, and K. Xu, “Unified gas-kinetic wave-particle methods I: Continuum and rarefied gas flow,” *Journal of Computational Physics* **401**, 108977 (2020).

<sup>13</sup>Z. Guo, R. Wang, and K. Xu, “Discrete unified gas kinetic scheme for all Knudsen number flows. II. Thermal compressible case,” *Physical Review E* **91**, 033313 (2015).

<sup>14</sup>Z. Guo and K. Xu, “Progress of discrete unified gas-kinetic scheme for multiscale flows,” *Advances in Aerodynamics* **3**, 6 (2021).

<sup>15</sup>M. H. Gorji, M. Torrilhon, and P. Jenny, “Fokker-Planck model for computational studies of monatomic rarefied gas flows,” *Journal of Fluid Mechanics* **680**, 574–601 (2011).

<sup>16</sup>M. Pfeiffer and M. Gorji, “Adaptive particle-cell algorithm for Fokker-Planck based rarefied gas flow simulations,” *Computer Physics Communications* **213**, 1–8 (2017).

<sup>17</sup>J. Mathiaud and L. Mieussens, “A Fokker-Planck Model of the Boltzmann Equation with Correct Prandtl Number,” *Journal of Statistical Physics* **162**, 397–414 (2016).

<sup>18</sup>H. Struchtrup and M. Torrilhon, “Regularization of Grad’s 13 moment equations: Derivation and linear analysis,” *Physics of Fluids* **15**, 2668–2680 (2003).

<sup>19</sup>J. Hu and R. Shu, “A Second-Order Asymptotic-Preserving and Positivity-Preserving Exponential Runge-Kutta Method for a Class of Stiff Kinetic Equations,” *Multiscale Modeling & Simulation* (2019), 10.1137/18M1226774.

<sup>20</sup>G. Dimarco and L. Pareschi, “Exponential Runge-Kutta Methods for Stiff Kinetic Equations,” *SIAM Journal on Numerical Analysis* (2011), 10.1137/100811052.

<sup>21</sup>W. Boscheri and G. Dimarco, “High order central WENO-Implicit-Explicit Runge Kutta schemes for the BGK model on general polygonal meshes,” *Journal of Computational Physics* **422**, 109766 (2020).

<sup>22</sup>Q. Li and L. Pareschi, “Exponential Runge-Kutta for the inhomogeneous Boltzmann equations with high order of accuracy,” *Journal of Computational Physics* **259**, 402–420 (2014).

<sup>23</sup>P. L. Bhatnagar, E. P. Gross, and M. Krook, “A Model for Collision Processes in Gases. I. Small Amplitude Processes in Charged and Neutral One-Component Systems,” *Physical Review* **94**, 511–525 (1954).

<sup>24</sup>E. M. Shakhov, “Generalization of the Krook kinetic relaxation equation,” *Fluid Dynamics* **3**, 95–96 (1968).

<sup>25</sup>S. M. Cox and P. C. Matthews, “Exponential Time Differencing for Stiff Systems,” *Journal of Computational Physics* **176**, 430–455 (2002).

<sup>26</sup>B. van Leer, “Towards the ultimate conservative difference scheme. II. Monotonicity and conservation combined in a second-order scheme,” *Journal of Computational Physics* **14**, 361–370 (1974).

<sup>27</sup>L. Zhu, Z. Guo, and K. Xu, “Discrete unified gas kinetic scheme on unstructured meshes,” *Computers & Fluids* **127**, 211–225 (2016).

<sup>28</sup>J. Y. Yang and J. C. Huang, “Rarefied Flow Computations Using Nonlinear Model Boltzmann Equations,” *Journal of Computational Physics* **120**, 323–339 (1995).

- <sup>29</sup>P. Wang, M. T. Ho, L. Wu, Z. Guo, and Y. Zhang, “A comparative study of discrete velocity methods for low-speed rarefied gas flows,” *Computers & Fluids* **161**, 33–46 (2018).
- <sup>30</sup>C. K. Chu, “Kinetic-Theoretic Description of the Formation of a Shock Wave,” *Physics of Fluids* **8**, 12 (1965).
- <sup>31</sup>G. Dechristé, *Méthodes numériques pour la simulation d’écoulements de gaz raréfiés autour d’obstacles mobiles*, Ph.D. thesis, Université de Bordeaux (2014).
- <sup>32</sup>C. Cercignani, *The Boltzmann Equation and Its Applications*, edited by F. John, J. E. Marsden, and L. Sirovich, Applied Mathematical Sciences, Vol. 67 (Springer New York, New York, NY, 1988).
- <sup>33</sup>C. Baranger, N. Hérouard, J. Mathiaud, and L. Mieussens, “Numerical boundary conditions in Finite Volume and Discontinuous Galerkin schemes for the simulation of rarefied flows along solid boundaries,” *Mathematics and Computers in Simulation* **159**, 136–153 (2019).
- <sup>34</sup>S. Fasoulas, C.-D. Munz, M. Pfeiffer, J. Beyer, T. Binder, S. Copplestone, A. Mirza, P. Nizenkov, P. Ortwein, and W. Reschke, “Combining particle-in-cell and direct simulation Monte Carlo for the simulation of reactive plasma flows,” *Physics of Fluids* **31**, 072006 (2019).
- <sup>35</sup>R. S. Myong, “A full analytical solution for the force-driven compressible Poiseuille gas flow based on a nonlinear coupled constitutive relation,” *Physics of Fluids* **23**, 012002 (2011).
- <sup>36</sup>K. Xu, “Super-Burnett solutions for Poiseuille flow,” *Physics of Fluids* **15**, 2077–2080 (2003).
- <sup>37</sup>U. Ghia, K. Ghia, and C. Shin, “High-Re solutions for incompressible flow using the Navier-Stokes equations and a multigrid method,” *Journal of Computational Physics* **48**, 387–411 (1982).
- <sup>38</sup>J.-C. Huang, K. Xu, and P. Yu, “A Unified Gas-Kinetic Scheme for Continuum and Rarefied Flows II: Multi-Dimensional Cases,” *Communications in Computational Physics* **12**, 662–690 (2012).